RSC Advances

PAPER

View Article Online
View Journal | View Issue

Cite this: *RSC Adv.*, 2020, **10**, 30650

Syntheses of four porous 3-D Cd(II) metal–organic frameworks from a new multidentate ligand 5-(imidazol-1-yl)-*N*′-(pyridin-4-ylmethylene) nicotinohydrazide and their characterization and adsorption properties†

Gui-Ying Zhu,‡[a] Zhenliang Liu,‡[b] Jia Wang,[a] Xue Niu,[a] Teng Wang,[a] Guo-Xia Jin*[a] and Jian-Ping Ma*[a]

Herein, a new multidentate ligand, 5-(imidazol-1-yl)-*N*′-(pyridin-4-ylmethylene) nicotinohydrazide (**L**), with an acylhydrazone group was synthesized and characterized. Subsequently, four porous Cd(II)-MOFs, *i.e.* $[Cd(L)(NO_3)]_n$ (**1**), $[Cd(L)Cl]_n$ (**2**), $[Cd(L)Br]_n$ (**3**), and $[Cd(L)I]_n$ (**4**), were assembled using the ligand **L** by a solvothermal method and characterized by single-crystal X-ray diffraction, infrared spectroscopy, thermogravimetric analysis, and powder X-ray diffraction. Structural analysis shows that the coordination environments around Cd(II) in all the four compounds are different due to the different coordinated anions. Among them, the coordination geometries and the arrangement of five-coordinated groups of the compound **1** containing the coordinated NO_3^- anions are significantly different from those of the other three compounds containing halides. However, all the four MOFs have similar one-dimensional rhombic channels. In these channels, both the nitrate ions and the halide ions are attached to the inner walls of the pores. The CO_2 adsorption properties of **1–4** were studied at 273 K, and the results showed that these compounds exhibit different adsorption capacities for CO_2 due to the presence of different ions in their pores.

Received 11th June 2020
Accepted 30th July 2020

DOI: 10.1039/d0ra05131d

rsc.li/rsc-advances

Introduction

In recent years, metal–organic frameworks (MOFs) have been extensively studied in the adsorption and separation of guest molecules, such as heavy metal ions,[1,2] chiral molecules,[3] dyes,[4] water,[5] and gases and volatile organic compounds,[6–10] due to their advantages of high porosity, low density, large surface area, regular channels, and tunable pore diameter. As is well-known, the pore size and functional interior environment of MOFs are the key factors determining the type of guest molecules adsorbed. Therefore, it is important to design and synthesize MOFs with suitable pore size and chemistry for the specific adsorption and separation of guest molecules. The pore size and interior surface of MOFs can be tuned and modified by changing the organic or inorganic building units *via* various ways, for example, changing the length and geometry of ligands,[11] introducing functional groups,[12,13] shifting counteranions,[9] using a mixed-ligand strategy,[14] and increasing the unsaturation sites of metal centers and improving the symmetry of inorganic core clusters.[15,16] Usually, the MOFs self-assembled from ligands containing multi-heteroatoms have better guest adsorption capacities due to weak host–guest interactions. For example, Zheng and co-workers have demonstrated that the MOFs synthesized from ligands containing acylamide groups have significantly improved CO_2 selective adsorption due to their enhanced CO_2 binding ability.[17] Dong and co-workers have reported that a Cd(II)-MOF constructed using a 4-amino-1,2,4-triazole-bridged ligand exhibits excellent adsorption and separation ability for aromatic, chlorocarbon, and C_2H_2 molecules because of its host–guest hydrogen-bonding interactions.[9,18,19] In this study, we designed and synthesized a new multidentate ligand, 5-(imidazol-1-yl)-*N*′-(pyridin-4-ylmethylene) nicotinohydrazide (**L**), with an acylhydrazide chelating group and two terminal coordination groups. Subsequently, four 3D porous Cd(II)-MOFs, $[Cd(L)(NO_3)]_n$ (**1**), $[Cd(L)Cl]_n$ (**2**), $[Cd(L)Br]_n$ (**3**), and $[Cd(L)I]_n$ (**4**), containing one-dimensional rhombic channels were synthesized by the self-assembly of the ligand **L** under solvothermal conditions and characterized by single-crystal X-ray

[a]*College of Chemistry, Chemical Engineering and Materials Science, Collaborative Innovation Center of Functionalized Probes for Chemical Imaging, Key Laboratory of Molecular and Nano Probes, Ministry of Education, Shandong Normal University, Jinan 250014, P. R. China. E-mail: xxgk123@163.com; guoxiajin@sdnu.edu.cn*

[b]*School of Chemistry and Pharmaceutical Engineering, Shandong First Medical University & Shandong Academy of Medical Sciences, Taian 271016, P. R. China*

† Electronic supplementary information (ESI) available. CCDC 1951144–1951147. For ESI and crystallographic data in CIF or other electronic format see DOI: 10.1039/d0ra05131d

‡ These authors contributed equally.

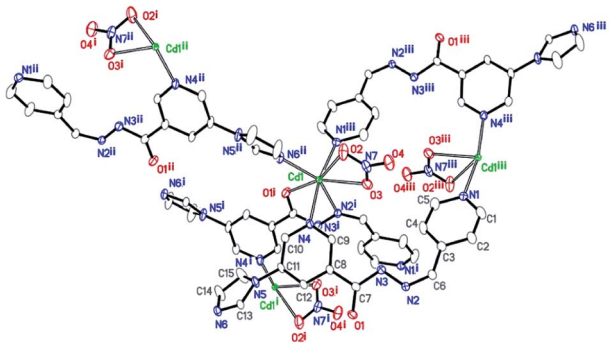

Fig. 1 Coordination environment of the Cd(II) centers in **1**, with displacement ellipsoids drawn at a 50% probability level [symmetry codes: (i): $-x, -y+1, -z+2$; (ii): $-x+1, y+1/2, -z+5/2$; and (iii): $x, -y+1/2, z+1/2$].

diffraction, infrared spectroscopy, thermogravimetric analysis, and powder X-ray diffraction. In addition, the CO_2 adsorption properties of the MOFs **1–4** were preliminarily studied.

Results and discussion

Crystal structure of the compound $[Cd(L)(NO_3)]_n$ (1)

Single-crystal X-ray diffraction analysis shows that the compound **1** crystallizes in the monoclinic space group $P2_1/c$. Its

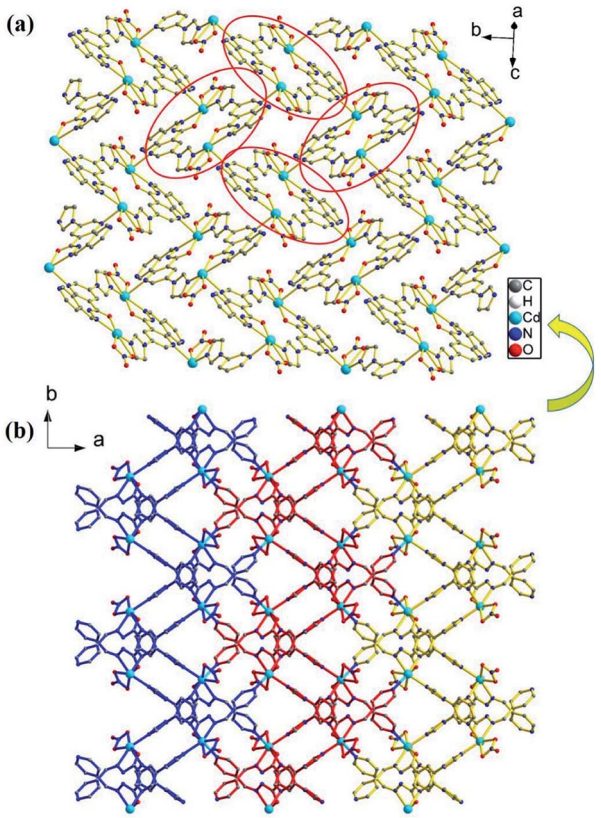

Fig. 2 (a) A 2D network containing two kinds of macrocycles with different axial positions viewed along the [302] crystallographic direction. (b) Parallel arrangement of the 2D networks along the *a*-axis, connected through Cd–$N_{pyridyl}$ bonds to form a 3D framework in **1**.

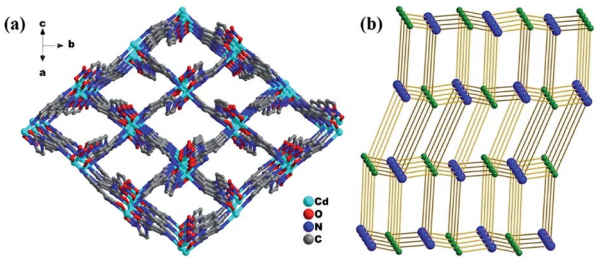

Fig. 3 (a) 3D framework of **1** and the rhombic channels viewed along the [101] crystallographic direction and (b) schematic of the (4,4)-connected pts network.

asymmetric unit contains one Cd(II) atom, one ligand **L**, and one nitrate anion (Fig. 1). Cd(II) lies in an irregular $[CdN_4O_3]$ pentagonal bipyramidal coordination environment. $N6^{ii}$, $O1^{i}$, $N2^{i}$, O3, and O2 from the imidazolyl and acylhydrazone chelating groups of the two ligands and one nitrate anion lie in the equatorial plane [Cd1–$N6^{ii}$ = 2.289(3), Cd1–$O1^{i}$ = 2.291(2), Cd1–$N2^{i}$ = 2.387(3), Cd1–O3 = 2.408(3), and Cd1–O2 = 2.638(3) Å]. The bond angles of $N6^{ii}$–Cd1–$O1^{i}$, $N2^{i}$–Cd1–O3, $N6^{i}$–Cd1–O2, and $O1^{i}$–Cd1–$N2^{i}$ are 82.62(10), 81.84(11), 76.80(10), and 69.37(10)°, respectively. Furthermore, two $N_{pyridyl}$ atoms from the terminal and di-substituted pyridyl groups of the other two ligands are located at the axial positions with the bond angles $N1^{iii}$–Cd1–N4, $N6^{ii}$–Cd1–N4, $N6^{ii}$–Cd1–$N1^{iii}$, $O1^{i}$–Cd1–N4, and $N6i^{i}$–Cd1–$O1^{i}$ being 169.46(10), 90.06(12), 99.51(12), 90.19(11), and 82.62(10)°, respectively. The bond lengths of Cd1–$N1^{iii}$ and Cd1–N4 are 2.332(3) and 2.425(3) Å, respectively. Moreover, two Cd(II) atoms are connected by the imidazolyl and acylhydrazone chelating groups of the two ligands [C7–O1 = 1.257(5), C7–N3 = 1.359(5), and C6–N2 = 1.277(5) Å] to form two kinds of 22-membered planar macrocycles with different axial positions (Fig. 2a). The dihedral angle between the two kinds of macrocyclic planes is *ca.* 77°. These two kinds of macrocyclic units are alternatively linked through Cd–N bonds between the Cd(II) atoms and di-substituted pyridyl nitrogen atoms to form a 2D network extending along the *bc* plane. The 2D nets are further parallelly connected by the Cd–N_1 bonds (N1 from the terminal pyridyl groups), as viewed down the crystallographic *c*-axis (Fig. 2b), to produce a 3D framework with 4,4-connected net nodes and pts topology (Fig. 3). Note that there exist 1D rhombic channels (cross section 12.18 Å × 13.52 Å), as viewed along the crystallographic [101] direction. The coordinated nitrate anions are located on the interior surface of the channels. Based on our previous study,[20] ligands containing monodentate and bidentate chelating binding sites can be very useful types of organic ligands for the construction of porous frameworks with high dimensionality. This result shows that the ligand **L** containing the imidazolyl and pyridyl terminal groups and acylhydrazone chelating binding sites can be an efficient organic linker for the construction of porous 3D frameworks.

Crystal structures of the compounds $[Cd(L)(X)]_n$ (2: X = Cl; 3: X = Br; and 4: X = I).

Compound **2** also crystallizes in the monoclinic space group $P2_1/c$. Single-crystal analysis shows that the compound **2** has

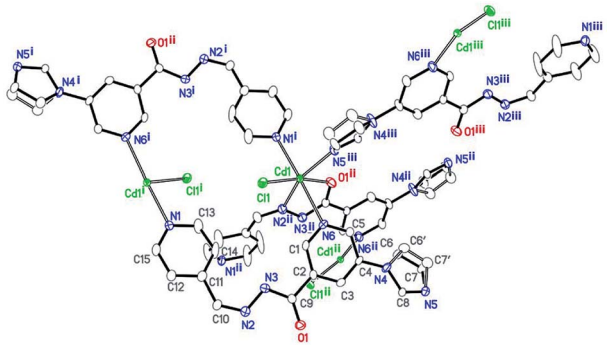

Fig. 4 Coordination environment of the Cd(II) centers in **2**, with displacement ellipsoids drawn at a 50% probability level [symmetry codes: (i): $-x+1, -y, -z$; (ii): $x, -y+1/2, z+1/2$; and (iii): $-x+2, y-1/2, -z+1/2$].

a similar 3D porous structure as **1**. As shown in Fig. 4, its asymmetric unit consists of one cadmium atom, one ligand, and one coordinated chloride ion. The Cd(II) center lies in a distorted octahedral environment. $N5^{iii}$, $O1^{ii}$, and $N2^{ii}$ from the imidazolyl group and acylhydrazone chelating group of the two ligands and Cl1 lie in the equatorial plane [Cd1–$N5^{iii}$ = 2.291(3), Cd1–$N2^{ii}$ = 2.358(3), Cd1–$O1^{ii}$ = 2.287(2), and Cd1–Cl1 = 2.4997(8) Å]. The bond angles of $O1^{ii}$–Cd1–$N5^{iii}$, $N5^{iii}$–Cd1–Cl1, $O1^{ii}$–Cd1–$N2^{ii}$, and $N2^{ii}$–Cd1–Cl1 are 86.04(9), 100.15(7), 69.91(9), and 103.32(7)°, respectively. In addition, two $N_{pyridyl}$ atoms ($N1^{i}$ and N6) from the terminal and di-substituted pyridyl groups of the other two ligands are located at the axial positions with the bond angle $N1^{i}$–Cd1–N6 being 176.71(9)°. The bond lengths of Cd1–$N1^{i}$ and Cd1–N6 are 2.403(3) and 2.500(3) Å, respectively. The bond angles of Cl1–Cd1–N6, $N5^{iii}$–Cd1–N6, $N2^{ii}$–Cd1–$N1^{i}$, $N5^{iii}$–Cd1–$N1^{i}$, are 89.81(7), 92.48(10), 95.49(10), and 90.69(10)°, respectively.

Similar to the case of **1**, every two Cd(II) atoms are connected by the imidazolyl and acylhydrazone chelating groups of the two ligands [C9–O1 = 1.257(2), C9–N3 = 1.348(2), and C10–N2 = 1.287(2) Å] to form a 22-membered planar macrocycles with

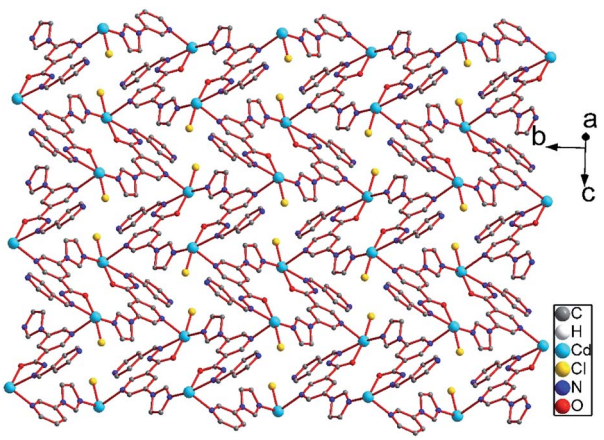

Fig. 5 2D network in **2** containing two kinds of macrocycles with different axial positions viewed along the [302] crystallographic direction.

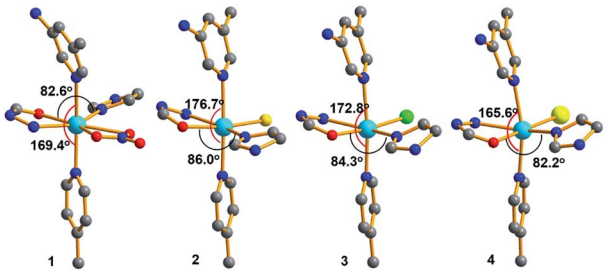

Fig. 6 Coordination environment around the Cd(II) centers in **1–4**.

different axial positions (Fig. 5). The dihedral angle between these two kinds of macrocyclic planes is *ca.* 66°. These two kinds of macrocyclic units are alternatively linked through Cd–N6 bonds between the Cd atoms and di-substituted pyridyl nitrogen atoms to form a 2D network extending along the *bc* plane. The 2D nets are further parallelly connected by Cd–N1 (N1 from the terminal pyridyl groups) bonds to yield a 3D porous framework with rhombic channels (cross section 13.86 Å × 14.19 Å), as viewed along the [101] crystallographic direction (Fig. S1 and S2†). Compared to the case of **1**, the coordinated chloride atoms are located on the interior surface of the channels in **2**.

When $CdBr_2$ and CdI_2 were used in the assembly reactions with the ligand **L**, the porous MOFs $[Cd(\mathbf{L})(Br)]_n$ (**3**) and $[Cd(\mathbf{L})(I)]_n$ (**4**) were obtained, which were allomeric with **2** (Fig. S3–S6†). Single-crystal analysis indicated that the Cd(II) centers lie in a similar distorted octahedral environment as in the case of **2**, except for the coordinated bromine and iodine atoms.

Further insights into the structures of **1–4** show that the coordination environments around Cd(II) in all the four compounds were different due to the different coordinated anions, as shown in Fig. 6. Among them, the coordination geometries and the arrangement of five-coordinated groups of the compound **1** containing coordinated NO_3^- are significantly different from those of the other three compounds containing halides. By comparison, the angles of N–Cd1–N located at the axial positions and O–Cd–N located at the equatorial positions decreased with an increase in the anion radius and size. The dihedral angles between the mono- and di-substituted pyridine rings also exhibited similar changes [**2**: 17.495°; **3**: 18.126°; **4**: 21.852°; and **1**: 21.973°]. Due to the difference in the Cd(II) coordination environments, the pore sizes of **1–4** also exhibit regular subtle changes; for example, the cross section areas are 12.18 Å × 13.52 Å (**1**), 13.86 Å × 14.19 Å (**2**), 13.72 Å × 14.15 Å (**3**), and 12.09 Å × 13.69 Å (**4**). Among them, the MOFs **1** and **4** with the biggest nitrate and iodine ions have the smallest channels, and the MOF **2** with the smallest chlorine ions has the biggest channels. Thus, in this study, the pore sizes and interior surfaces of the Cd(II)-MOFs could be tuned by changing the anions.

IR, TGA and PXRD

Infrared (IR) spectra of the compounds **1–4** (Fig. S7†) show strong absorption peaks around 1666 cm^{-1}, which are

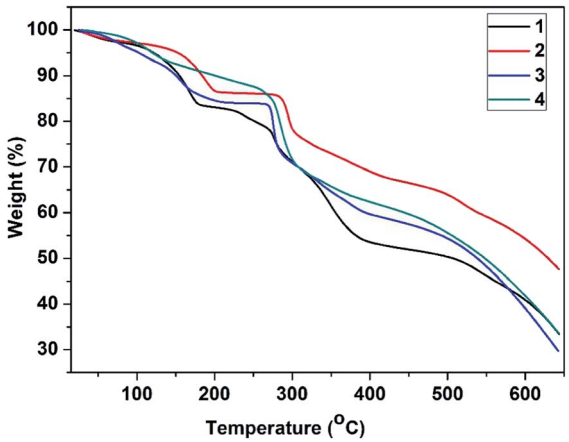

Fig. 7 TGA curves of **1–4**.

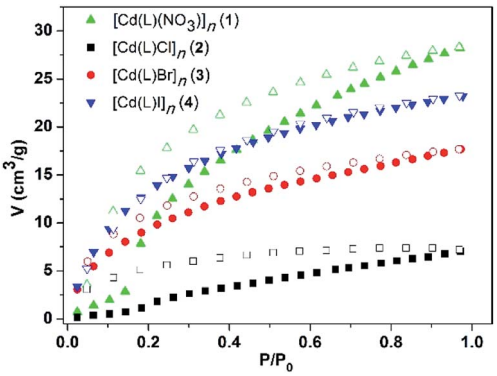

Fig. 8 CO_2 adsorption isotherm curves of the MOFs **1–4** at 273 K.

attributed to the C=O stretching vibration of the acylhydrazone group; the peaks around 1590 cm^{-1} can be attributed to the C=N stretching vibration of pyridyl groups; the peak around 1330 cm^{-1} corresponds to the N–N stretching vibration of the acyl hydrazone group.

Thermogravimetric analysis (TGA) curves shown in Fig. 7 reveal that the frameworks of **1–4** have similar thermal stabilities. All the four MOFs were stable up to around 270 °C, after which they began to decompose. The compounds **1–3** underwent the first weight loss in the temperature range from 25 to 200 °C due to the loss of the guest DMF molecules, which were confirmed to be present in the MOFs by an ^1H NMR spectrum (Fig. S8†), and the framework started to disintegrate at *ca.* 270 °C. In the case of the compound **4**, these encapsulated DMF molecules were removed at temperatures ranging from 25 to 270 °C, and then, the framework began to decompose.

The room-temperature powder X-ray diffraction (PXRD) patterns of **1–4** are shown in Fig. S9.† All the peaks in the obtained curves approximately match those in the simulated curves generated based on the single-crystal diffraction data; this confirms the phase purity of the as-prepared products.

CO_2 adsorption properties of the MOFs 1–4

Considering the existence of 1D channels, the CO_2 adsorption measurements were performed for the desolvated MOFs **1–4**. Before measurement, the as-synthesized crystal samples of **1–4** were immersed in methanol to exchange the uncoordinated DMF molecules. Then, drying was conducted at 60 °C under high vacuum for 3 h to obtain activated samples.

The adsorption isotherm curves of the MOFs **1–4** for CO_2 were measured, and the MOFs **3** and **4** exhibited typical type-I isotherms and the adsorption curves were in agreement with the desorption curves at 273 K, as shown in Fig. 8. However, the other two MOFs, especially the MOF **1**, displayed a sharp adsorption increase at one point upon increasing the pressure. This phenomenon indicated that the MOFs might undergo subtle structural changes and the windows of the channels suddenly open; this might also have resulted in the hysteretic phenomenon of their desorption curves. The adsorption isotherms suggest that the CO_2 sorption capacity is 6.80 $cm^3\ g^{-1}$ for **2**, 17.67 $cm^3\ g^{-1}$ for **3**, 23.27 $cm^3\ g^{-1}$ for **4**, and 28.30 $cm^3\ g^{-1}$ for **1**, which are close to those of some of the reported MOFs such as ZIF-95 (19.7 $cm^3\ g^{-1}$) and ZIF-8 (32.22 $cm^3\ g^{-1}$).[21,22] The BET surface areas of **1–4**, calculated according to their CO_2 adsorption isotherms, are 266.54, 164.10, 151.26, and 165.42 $m^2\ g^{-1}$, respectively. In particular, the Cd-MOFs **1** and **4** with bigger nitrate and iodine ions are beneficial for the adsorption of CO_2 than **2** with a smaller chloride ion. These results show that the anions attached to the frameworks have an effect on the adsorption ability of the Cd-MOFs. The CO_2 uptake capacity gradually increases with an increase in the size of the anion. This is probably because different anions change the pore volumes differently such that the pores with larger anions better match the CO_2 molecules. On the other hand, the I^- anion has bigger polarizability than Cl^- and Br^-, and NO_3^- has more N–O polar bonds. Thus, the lone pairs of the more polarizable I atom or electronegative O atom may interact with the electropositive C atom of CO_2; this would probably lead to better sorption capacity of the MOFs containing I^- and NO_3^- anions than those of the MOFs with Cl^- and Br^-.[23] Overall, the pore sizes are substantially large as compared to the adsorbed gas molecules; therefore, the sorption capacities of all the four MOFs are relatively low.

Experimental

General methods

All reagents were used as purchased without further purification. IR spectra were obtained by a BIO-RAD FTS-40 Infrared Spectrometer (KBr pellet). TGA was conducted using a TA instrument, Q5 series thermogravimetric analyzer, at the heating rate of 10 °C min^{-1}. Powder X-ray diffraction was carried out by a Bruker powder diffractometer with Cu Kα radiation as the X-ray source and the scanning angle of 2-theta = 5–50°. Photoluminescence was determined by an FLS-920 fluorescence analyzer.

Synthesis of the ligand

Synthesis of 5-imidazolyl nicotinic acid. 5-Bromonicotinic acid (3.0 g, 15.0 mmol), imidazole (1.4 g, 21.0 mmol), cuprous

iodide (0.6 g, 3.0 mmol), and cesium carbonate (14.5 g, 45.0 mmol) were added to a 250 mL three-necked bottle containing 15 mL *N*,*N*-dimethylformamide (DMF) under a N_2 atmosphere. After being heated at 120 °C for 24 h, the reaction mixture was poured into 200 mL of water and filtered. The filtrate was acidified to pH = 5 and then filtered. The filtrate was concentrated to 1/4 of the original volume to produce solids followed by filtration and drying. Finally, 5-imidazolyl nicotinic acid was obtained (yield, 81%).

Synthesis of 5-imidazolyl methyl nicotinate. A round-bottom flask was charged with 5-imidazolyl nicotinic acid (1.0 g, 5.0 mmol) and methanol (20 mL); then, 2 mL of concentrated sulfuric acid was added dropwise to the abovementioned solution. The solution was stirred under reflux for 4–5 h. After completion of the reaction, the solution was cooled down to room temperature, poured into 100 mL of water, and further cooled in an ice water bath. After adjusting the pH of the resulting solution to 7 using aqueous Na_2CO_3, crude 5-imidazolyl methyl nicotinate was acquired by filtration followed by drying and further purification by silica gel column chromatography to obtain pure 5-imidazolyl methyl nicotinate (0.9 g, yield 88%).

Synthesis of 5-imidazolyl nicotinic acid hydrazide. 5-Imidazolyl methyl nicotinate (2.0 g, 10.0 mmol) was dissolved in 20 mL of ethanol in a 100 mL round-bottom flask, and then, a solution of excess of $N_2H_4 \cdot H_2O$ (5.7 mL, 100 mmol) in ethanol (10 mL) was added dropwise to the abovementioned solution. The mixture was heated to reflux, and the reaction was detected by TLC. After completion of the reaction, the mixture was cooled down and filtered to remove the yellow solid by-products. A white solid was precipitated from the filtrate, which was washed three times with diethyl ether to obtain a white solid (1.8 g, yield 92%).

Synthesis of 5-(imidazol-1-yl)-*N*′-(pyridin-4-ylmethylene) nicotinohydrazide (L). 5-Imidazolyl nicotinic acid hydrazide (0.5 g, 2.5 mmol), 4-pyridinecarboxaldehyde (0.32 g, 3.0 mmol), anhydrous ethanol (10 mL), and formic acid (0.1 mL) were added to a round-bottom flask followed by refluxing for 24 h. The reaction solution was cooled and filtered. The solid was completely washed with absolute ethanol and dried to acquire a white solid (0.64 g, yield 90%).

Synthesis of the MOFs

Synthesis of compound 1. **L** (3.0 mg, 0.01 mmol), $Cd(NO_3)_2$ (2.4 mg, 0.03 mmol), and DMF (2 mL) were placed in a 5 mL test tube and sealed. The reaction mixture was maintained at 90 °C for three days. After cooling the resulting mixture to room temperature for two days, 2.1 mg dark yellow crystals were obtained with a yield of 45%. IR (KBr pellet, cm^{-1}): 3133 (w), 3105 (w), 1668 (s), 1588 (s), 1520 (s), 1388 (m), 1331 (s), 1068 (m).

Synthesis of compound 2. Compound **2** was synthesized by the same process as that used for compound **1** except that $CdCl_2$ (5.4 mg, 0.03 mmol) was used instead of $Cd(NO_3)_2$, and 1.5 mg yellow crystals were obtained with a yield of 34%. IR (KBr pellet, cm^{-1}): 3121 (w), 1658 (s), 1590 (m), 1513 (s), 1390 (m), 1336 (s), 1004 (s).

Synthesis of compound 3. Compound **3** was synthesized by the same process as that used for compound **1** except that $CdBr_2$ (8.1 mg, 0.03 mmol) was used instead of $Cd(NO_3)_2$, and 3.5 mg pale yellow crystals with a yield of 72% were obtained. IR (KBr pellet, cm^{-1}): 3133 (w), 1674 (s), 1599 (m), 1519 (s), 1385 (m), 1341 (s), 1068 (m), 1004 (m).

Synthesis of compound 4. Compound **4** was synthesized by the same process as that used for compound **1** except that CdI_2 (10.8 mg, 0.03 mmol) was used instead of $Cd(NO_3)_2$, and 2.6 mg dark yellow crystals with a yield of 50% were acquired. IR (KBr pellet, cm^{-1}): 3133 (w), 3041 (w), 1674 (s), 1599 (m), 1519 (s), 1341 (s), 1068 (m), 1004 (m).

Refinement

For **1**: the hydrogen atoms attached to carbon atoms were placed in geometrically idealized positions and refined using a riding model with C–H = 0.93 (aromatic) and $U_{iso}(H) = 1.2U_{eq}(C)$ for all H atoms. A large void space is present in the framework, which exhibits many significant electron density peaks. The species were too severely disordered to be modeled and were treated with SQUEEZE/PLATON. The solvent-accessible void volume calculated by this program was 812 $Å^3$ (35.4% of the total unit cell volume (2291.8(2) $Å^3$)), corresponding to 264 e^- per cell. These species include some DMF and H_2O molecules.

For **2**: the atoms C_6 and C_7 of the imidazole ring are disordered over two orientations, with refined site occupation factors of 0.46(5) : 0.54(5). A large void space is present in the framework, and the species were too severely disordered to be modeled. Therefore, they were treated with SQUEEZE/PLATON, and the solvent-accessible void volume calculated by this program was 758 $Å^3$ (34.2% of the total unit cell volume (2219.14(9) $Å^3$)), corresponding to 228 e^- per cell. These species include some DMF and H_2O molecules.

For **3**: all non-hydrogen atoms were refined with anisotropic displacement parameters. The hydrogen atoms attached to carbon atoms were placed in geometrically idealized positions and refined using a riding model with C–H = 0.93 (aromatic) and $U_{iso}(H) = 1.2U_{eq}(C)$ for all H atoms. The atoms C_6 and C_7 of the imidazole ring are disordered over two orientations, with the refined site occupation factors of 0.48(8) : 0.52(8). A large void space is present in the framework, which exhibits many significant electron density peaks. The species were too severely disordered to be modeled and were treated with SQUEEZE/PLATON. The solvent-accessible void volume calculated by this program was 721 $Å^3$ (31.9% of the total unit cell volume (2262.9(2) $Å^3$)), corresponding to 231 e^- per cell. These species include some DMF and H_2O molecules. The contribution of the disordered species was removed from the structure factor calculations. The tabulated *F*(000), MW, and density reflect known cell contents only.

For **4**: The hydrogen atoms attached to carbon atoms were placed in geometrically idealized positions and refined using a riding model with C–H = 0.93 (aromatic) and $U_{iso}(H) = 1.2U_{eq}(C)$ for all H atoms. A large void space is present in the framework, and the species were too severely disordered to be

modeled and were treated with SQUEEZE/PLATON. The solvent-accessible void volume calculated by this program was 810 $Å^3$ (35.4% of the total unit cell volume (2284.1(2) $Å^3$)), corresponding to 281 e^- per cell. These species include some DMF and H_2O molecules.

Gas adsorption measurements

The CO_2 sorption isotherms were measured using an automatic volumetric adsorption apparatus (Quantachrome Autosorb-IQ-MP) at 273 K. Before gas adsorption testing, the as-synthesized compounds **1–4** were placed in renewed methanol for one day (three times) in order to totally remove the DMF molecules. The samples were activated by drying in a vacuum oven at 90 °C for 30 min. Before measurement, the activated samples were dehydrated again *via* the "outgas" function of the adsorption analyzer for 3 h at 80 °C.

Conclusions

In this study, a new multidentate ligand, 5-(imidazol-1-yl)-*N*′-(pyridin-4-ylmethylene) nicotinohydrazide (**L**), with an acylhydrazide group was synthesized and characterized. Subsequently, four porous Cd(II)-MOFs, $[Cd(\mathbf{L})(NO_3)]_n$ (**1**), $[Cd(\mathbf{L})Cl]_n$ (**2**), $[Cd(\mathbf{L})Br]_n$ (**3**) and $[Cd(\mathbf{L})I]_n$ (**4**), were assembled using the ligand **L** by a solvothermal method and characterized by single-crystal X-ray diffraction, infrared spectroscopy, thermogravimetric analyses, and powder X-ray diffraction. Structural analysis shows that the coordination environments around Cd(II) in all the four compounds were different due to the different coordinated anions. Among them, the coordination geometries and the arrangement of five-coordinated groups of the compound **1** containing the coordinated NO_3^- anions are significantly different from those of the other three compounds containing halides. However, all four MOFs have similar one-dimensional rhombic channels. In these channels, both nitrate ions and halide ions are attached on the inner walls of the pores. The CO_2 adsorption properties of **1–4** were studied at 273 K, and the results showed that these compounds exhibit different adsorption capacities for CO_2 due to different ions in their pores. Further research on the adsorption properties of this type of Cd-MOFs for other guests is underway.

Conflicts of interest

The authors declare no competing financial interest.

Acknowledgements

We acknowledge the financial support provided by NSFC (Grant No. 21771120).

Notes and references

1 Z. H. Yang, J. Cao, Y. P. Chen, X. Li, W. P. Xiong, Y. Y. Zhou, C. Y. Zhou, R. Xu and Y. R. Zhang, *Microporous Mesoporous Mater.*, 2019, **277**, 277–285.
2 Y. Wu, Y. Ma, G. Xu, T. Xia, W. Liu, Z. Dong, Q. Yuan, C. Zhang and Q. J. Hu, *Mater. Sci.*, 2019, **54**, 2093–2101.
3 D. Balestri, D. Capucci, N. Demitri, A. Bacchi and P. Pelagatti, *Materials*, 2017, **10**, 727.
4 D. Jiang, M. Chen, H. Wang, G. Zeng, D. Huang, M. Cheng, Y. Liu, W. Xue and Z. Wang, *Coord. Chem. Rev.*, 2019, **380**, 471–483.
5 H. Kim, S. Yang, S. R. Rao, S. Narayanan, E. A. Kapustin, H. Furukawa, A. S. Umans, O. M. Yaghi and E. N. Wang, *Science*, 2017, **356**, 430–434.
6 X. Wang, Y. Wu, J. Peng, Y. Wu, J. Xiao, Q. Xia and Z. Li, *Chem. Eng. J.*, 2019, **358**, 1114–1125.
7 P. Q. Liao, N. Y. Huang, W. X. Zhang, J. P. Zhang and X. M. Chen, *Science*, 2017, **356**, 1193–1196.
8 N. Thi, X. Huynh, V. Chihaia and D. N. Son, *J. Mater. Sci.*, 2019, **54**, 3994–4010.
9 G. X. Jin, X. Niu, J. Wang, J. P. Ma, T. L. Hu and Y. B. Dong, *Chem. Mater.*, 2018, **30**, 7433–7437.
10 G. X. Jin, J. Wang, J. Y. Liu, J. P. Ma and Y. B. Dong, *Inorg. Chem.*, 2018, **57**, 6218–6221.
11 V. Guillerm, D. Kim, J. F. Eubank, R. Luebke, X. Liu, K. Adil, M. S. Lah and M. Eddaoudi, *Chem. Soc. Rev.*, 2014, **43**, 6141–6172.
12 Y. B. Zhang, H. Furukawa, N. Ko, W. Nie, H. J. Park, S. Okajima, K. E. Cordova, H. Deng, J. Kim and O. M. Yaghi, *J. Am. Chem. Soc.*, 2015, **137**, 2641–2650.
13 Z. Lu, F. Meng, L. Du, W. Jiang, H. Cao, J. Duan, H. Huang and H. He, *Inorg. Chem.*, 2018, **57**, 14018–14022.
14 B. Liu, H. F. Zhou, L. Hou and Y. Y. Wang, *Dalton Trans.*, 2018, **47**, 5298–5303.
15 I. Bratsos, C. Tampaxis, I. Spanopoulos, N. Demitri, T. A. Steriotis and P. N. Trikalitis, *Inorg. Chem.*, 2018, **57**, 7244–7251.
16 J. Jiang, Z. Lu, M. Zhang, J. Duan, W. Zhang, Y. Pan and J. Bai, *J. Am. Chem. Soc.*, 2018, **140**, 17825–17829.
17 B. Zheng, J. Bai, J. Duan, L. Wojtas and M. J. Zaworotko, *J. Am. Chem. Soc.*, 2011, **133**, 748–751.
18 Q. K. Liu, J. P. Ma and Y. B. Dong, *J. Am. Chem. Soc.*, 2010, **132**, 7005–7017.
19 Q. K. Liu, J. P. Ma and Y. B. Dong, *Chem. Commun.*, 2011, **47**, 12343.
20 X. W. Wu, F. Pan, D. Zhang, G. X. Jin and J.-P. Ma, *CrystEngComm*, 2017, **19**, 5864–5872.
21 A. Phan, C. J. Doonan, F. J. Uribe, C. B. Knobler, M. O. Keeffe and O. M. Yaghi, *Acc. Chem. Res.*, 2010, **43**, 58–67.
22 J. W. Maina, P. G. Cristina, J. A. Schütz, J. T. Wang and L. F. Dumee, *Carbon*, 2019, **148**, 80–90.
23 R. Vaidhyanathan, S. S. Iremonger, G. K. H. Shimizu, P. G. Boyd, S. Alavi and T. K. Woo, *Science*, 2010, **330**, 650–653.